J. Fish. Sci. Tech. 1(1), 7~18, 1998

Numerical Experiment on the Sogcho Eddy due to the strong offshore winds in the East Sea

Soon Young Kim, Hyong Sun Lee and Jae Chul Lee[1]*

Department of Oceanography, Korea Naval Academy, Chinhae 645-797, Korea

[1]Department of Oceanography, Pukyong National University, Pusan, 608-737, Korea

(Received November 1997, Accepted June 1998)

In order to understand the generation of the Sogcho Eddy due to the strong offshore winds, we first investigated the characteristics of winds at Sogcho, Kangnung and Samchuk, and then carried out a series of numerical experiments using the nonlinear 1 ½-layer model. The models were forced by wind stress fields, similar in structure to the prevailing winds that a field in the east coast of Korea during the winter season. The winds were composed of the background winds (~1 dyne/cm^2) for 90 days and the local winds (~4 dyne/cm^2) for 30 days.

The analysis of wind data at three stations (Sogcho, Kangnung, and Samchuk) showed that the wind was stronger in winter than in other seasons and the offshore component was much dominant. According to our numerical solutions, the Sogcho Eddy of about 200 km in diameter was generated due to the strong offshore winds prevailing in the Kangnung - Sogcho regions. The eastward propagation of the Rossby waves reflected at the western boundary resulted in the eastward meandering motion from the eastern side of the eddy.

Key words: Sogcho eddy, offshore winds, nonlinear 1 ½-Layer model, rossby waves, meandering, conservation of potential vorticity, entrainment

Introduction

In general, the wavelength of a disturbance calculated according to the baroclinic instability is in good agreement with eddies generated in the open ocean or the western boundary current regions. For the Sogcho Eddy, the internal Rossby radius is about 15 km yielding the wavelength of the unstable Rossby wave of about 100 km (Lee et al., 1995). However, the size of the Sogcho Eddy of about 200 km is twice as large as that generated by the baroclinic instability theory. Consequently, other generating factors may have played an important role in the generation of the Sogcho Eddy in addition to the baroclinic instability. Lee et al. (1995) suggested that the strong offshore winds off the east coast of Korea might exert significant influence because the Sogcho Eddy is generated mostly in winter.

Na et al. (1992) studied the mean sea surface winds over the adjacent seas of Korea. The northerly and northwesterly winds were dominant over the East Sea in winter. In particular, the wind stress of about 1.0 dyne/cm^2 appeared over the entire East Sea from December through February, and its maximum value exceeded 2.2 dyne/cm^2 in January. While the northerly wind prevailed in the northern part of 40°N in winter, the northwesterly wind dominated in the southern part. Choi and Lee (1993) proposed that the predominant wind in Sogcho region was the northwesterly wind in January, February and March, and the westerly and northwesterly winds in September and December. According to these results, the northwestly or westly winds seemed to be considerably strong at the east coast of Korea in winter.

The offshore winds off the east coast of Korea are very strong in winter season and this wind system is believed to be one of the possible mechanism for eddy generation. Thus, we first analyzed the wind data at Sogcho, Kangnung and Samchuk, and then investigated the effect of the strong offshore winds on the generation of the Sogcho Eddy using the nonlinear 1 ½ - layer model.

The Wind Data

The hourly wind data at Sogcho, Kangnung and Samchuk for 5 years from January 1, 1988 to

*To whom correspondence should be addressed.

December 31, 1992 were analyzed. The local coordinate system was rotated 30°west of true north to obtain the alongshore and offshore components of wind velocity.

Fig. 1 shows the low-pass filtered time series of the offshore and alongshore components of wind velocity at Sogcho (a), Kangnung (b) and Samchuk (c). A low-pass filter with cut-off frequency of 0.02 cycle per hour was applied to eliminate any higher frequency variability. The positive values of the offshore and alongshore components correspond to ENE and NNW direction, respectively. The winds at three stations are much stronger in winter season than in other seasons. The offshore component is especially strong from January through February, and it weakens from June to September and begins to strengthen again from October to December. The variation patterns are very similar at all three stations. The alongshore component is particularly weaker than the offshore component at Kangnung. The offshore component as well as the alongshore component at Samchuk is weaker than at Sogcho and Kangnung during the whole period, but it is noted that the offshore component reaches about 10 m/sec in the onshore direction from January to May in 1992. The offshore component at Sogcho and Kangnung with 5 m/sec from January to mid February in 1988 and 1992 is stronger than in any other year.

Fig. 2 shows the spectral density of the hourly wind at Sogcho (a), Kangnung (b) and Samchuk (c) for 5 years. The spectra at three stations have essentially the same trend; the first significant peak appears at about 1.0 cycle per day (cpd) corresponding to the land-sea breeze with diurnal period. The second significant peak at about 2.0 cpd can not be explained now. In addition to these significant peaks, the other significant peaks also appear at about 0.01 cpd and 0.05 cpd which contain the dominant portion of the wind energy.

Both offshore and alongshore components at Sogcho are almost the same, and the variability at 0.01 cpd is larger than any other peak in the frequency band lower than 0.1 cpd. Whereas the offshore component is large at low frequency, the alongshore component is large at high frequency (Fig. 2a). The offshore component at Kangnung is about ten times stronger than the alongshore component in all frequency ranges (Fig. 2b). The offshore component at Samchuk is stronger than the alongshore component in all the frequency ranges as in Kangnung, but the major significant peak appears at 0.01 cpd as in Sogcho (Fig. 2c).

In summary, the significant peaks are at 1.0 cpd (diurnal period) and 2.0 cpd (semi-diurnal period), but a synoptic band between 0.05 cpd and 0.01 cpd contains the dominant portion of the wind energy. The offshore component is stronger than the alongshore component at both Sogcho and Kangnung in winter season. The wind at Samchuk is weaker than at Sogcho and Kangnung. In particular, the offshore component at Sogcho and Kangnung from December 1991 through February 1992 is much more stronger than in any other year. It is sure that these offshore winds are strong enough to influence the generation of the Sogcho Eddy in winter season.

The Model Oceans

1. Model description

The nonlinear 1 ½ - layer model used in this study is basically the same as our previous numerical study (Kim et al., 1997a,b). As a result, the momentum and governing equations are the same as those of the polar front study, but the wind stress terms (τ^x, τ^y) are included in momentum equations in this offshore winds study.

Boundary conditions, model parameters and numerical methods are the same as those in the previous numerical studies (Kim et al., 1997a,b). However, the model domain is different because the main interest of this study is to investigate the Sogcho Eddy off the east coast of Korea. The model domain is 600 km in zonal direction (Fig. 3). The southern and eastern boundaries are assumed to be artificially open.

2. Wind forcing

In this offshore winds study, the model ocean is forced by wind fields similar in strength and structure to the winds over the East Sea in winter season. The wind fields have separable forms

$$\tau^x = \tau_0 X(x) Y(y) \mathcal{T}(t)$$
$$\tau^y = -\tau_0 X(x) Y(y) \mathcal{T}(t),$$

where τ^x and τ^y are the offshore and alongshore components, respectively. The negative sign (−) means the northerly wind and X, Y and $\mathcal{T}$ are the offshore, alongshore and temporal structure of wind fields, respectively. For the determination of spatial - temporal structure of wind fields used in this

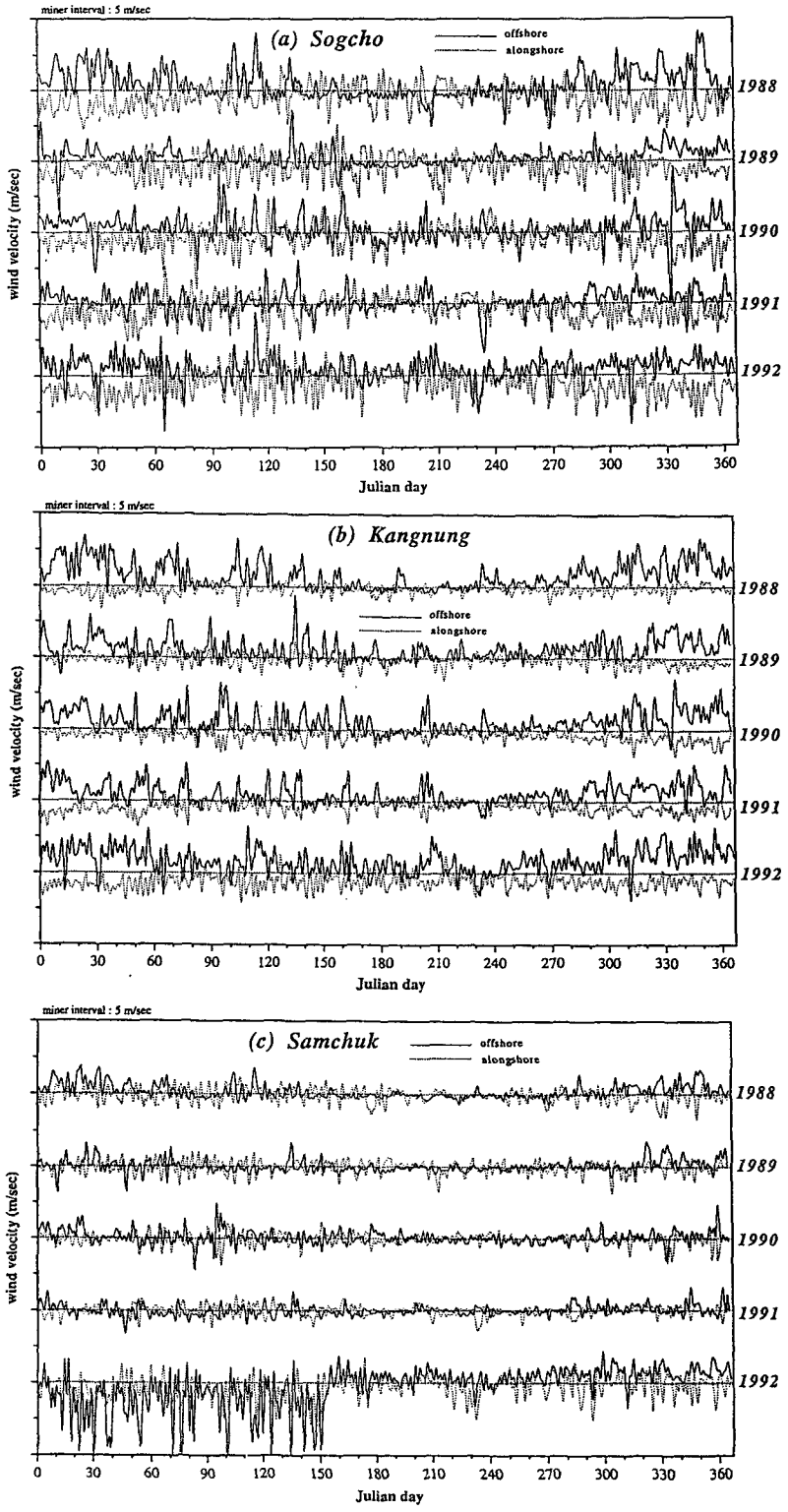

Fig. 1. Time series of offshore and alongshore components of hourly wind data with 50 - hour low - pass filtered at Sogcho (a), Kangnung (b) and Samchuk (c).

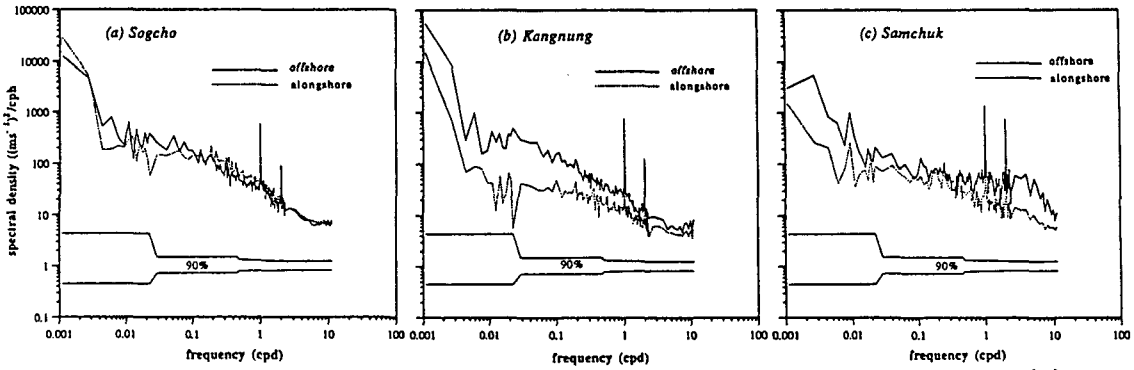

Fig. 2. Autospectra of offshore and alongshore components of hourly wind data at Sogcho (a), Kangnung (b) and Samchuk (c).

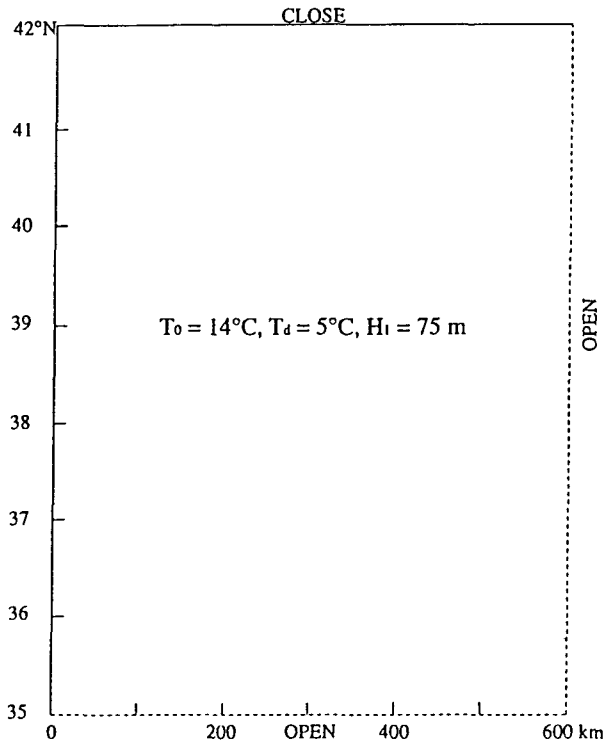

Fig. 3. The model ocean illustrating the model domain and initial conditions.

model, the results of wind data analysis in the present study and the distribution pattern of winds in the East Sea from the analysis by Na et al. (1992) were referred.

Fig. 4 illustrates the wind fields that forces the model ocean in the offshore winds study. It shows the locations of the wind fields as well as their spatial and temporal structures, $X(x)$, $Y(y)$ and $T(t)$. The wind fields have three components; a background wind field τ^x_B in the offshore direction, τ^y of alongshore winds that represents the moderate northerly and the northwesterly wind in winter season, and offshore winds patch τ^x_J. The maximum value of wind stress in the background wind field τ^x_B is 1 dyne/cm^2 at 39°N, it decreases smoothly both to the south and north relative to 39 °N, and goes to zero at the northern and southern boundaries. The background wind is cut off near the eastern boundary in the offshore distance. The northerly wind stress has the magnitude of 1 dyne /cm^2 between 42°N and 40°N, then decreases gradually southward and becomes zero at 38°N. In addition, it is essentially uniform to the offshore distance (Fig. 4a). The winds patch τ^x_J with 2° in the alongshore distance centered at 39° has a maximum value of 4 dyne/cm^2 and decreases gradually offshore to 250 km. Therefore, the total wind stress field ($\tau^x_B+\tau^y+\tau^x_J$) which represents wind pattern during the peak phase of the northwest monsoon, is shown in Fig. 4b. Fig. 4c shows the temporal structure $T(t)$ of the maximum strength variation of τ^x_B, τ^y and τ^x_J, with $t=0$ corresponding to December 1. Temporal structures $T(t)$ of τ^y and background wind fields τ^x_B increase smoothly for the first 15 days, and remain constant after 15 days until 75 days, and then they relax to zero from day 75 to 90. $T(t)$ of the winds patch τ^x_J increases smoothly from day 15 to 20, and it keeps constant after 20 days until 40 days, and then it relaxes to zero from day 40 to 45. The maximum value of wind stress is, therefore, about 5 dyne/cm^2 at the 39 °N from day 20 to 40.

Numerical Results

As shown in section 2, the offshore winds were considerably stronger in the vicinity of Sogcho in winter season. Since strong wind forcing is believed as one of the possible eddy generation mechanisms, the wind effect on the generation of the Sogcho Eddy were investigated in this offshore winds

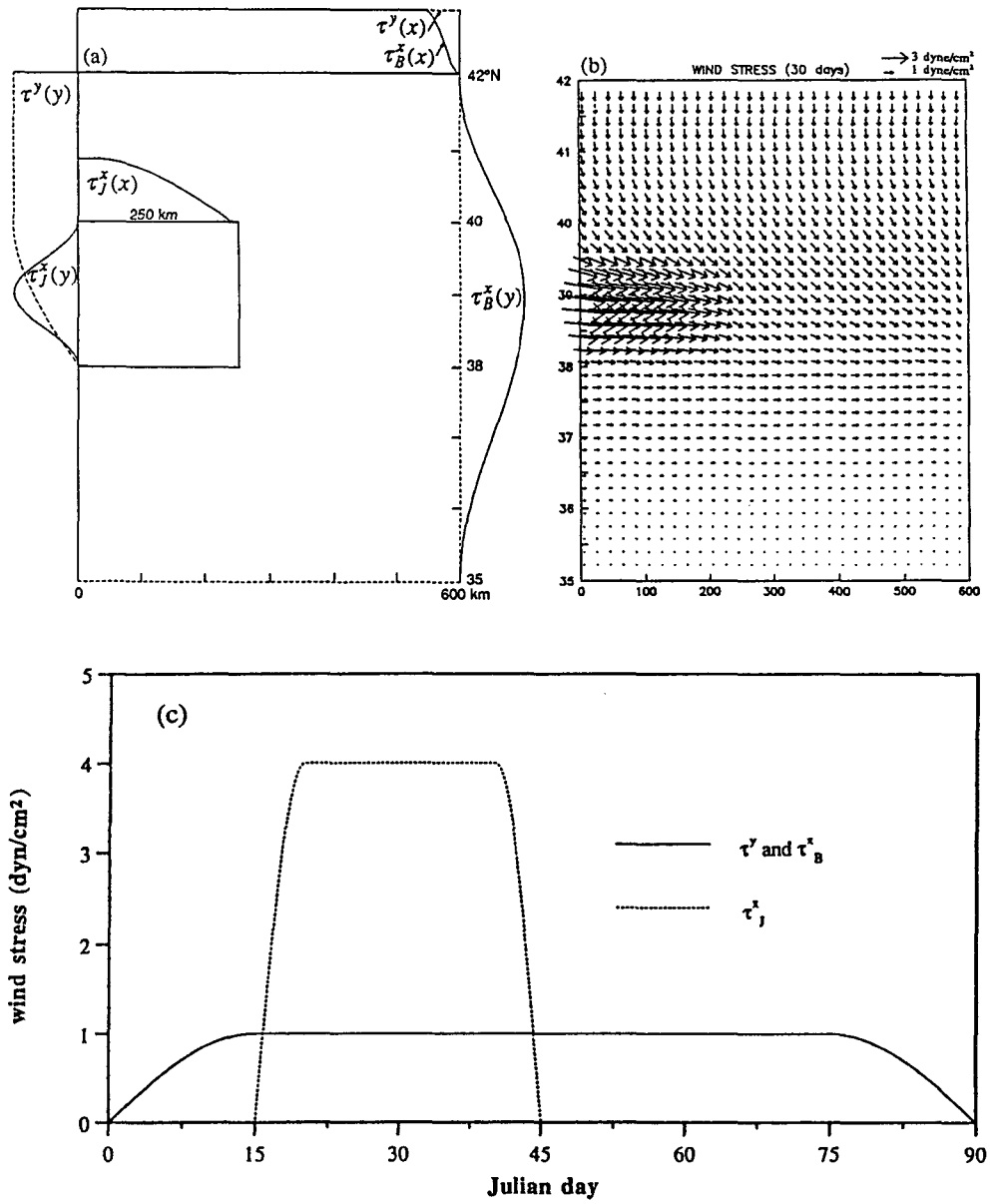

Fig. 4. A schematic diagram illustrating the spatial (a, b) and temporal (c) structure of the wind field.

study using the nonlinear 1½ - layer model. The model ocean was forced by offshore and alongshore winter winds for 90 days, but the initial state of the model ocean was assumed to be motionless.

At day 15 (Fig. 5), southward current is developing along the northern and western boundaries due to the northerly wind and its speed reaches about 10~11 cm/sec (Fig. 5a). This southward coastal current disappears after day 90 as the northerly wind decays. The deepening of the *h* -field to the right of the current in Fig. 5b is explained by the thermal wind relation. Maximum values of the h-field reaches about 87 m at the right side of the southward coastal current along the western boundary.

According to the various additional numerical calculations, the southward current speed caused by the northerly wind increased to over 15 cm/sec when the wind τ^y (τ_0) increased to -3 dyne/cm^2, but the southward current did not influence the features of the interior flow produced by the westerly wind because the southward coastal current disappeared as soon as the northerly wind decayed.

At day 30 (Fig. 6), an anticyclonic eddy develops due to the strong offshore winds on the right side of the wind axis between 38°N and 39°N. Its

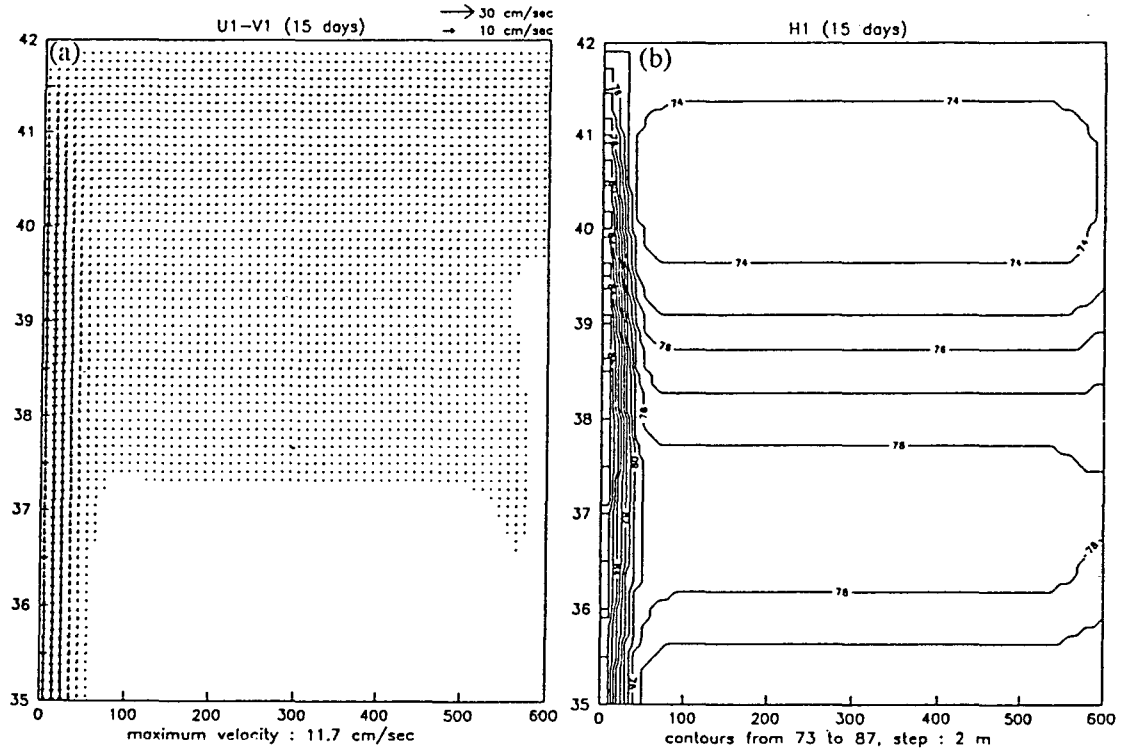

Fig. 5. A current field (a) and h field (b) of the upper layer at day 15.

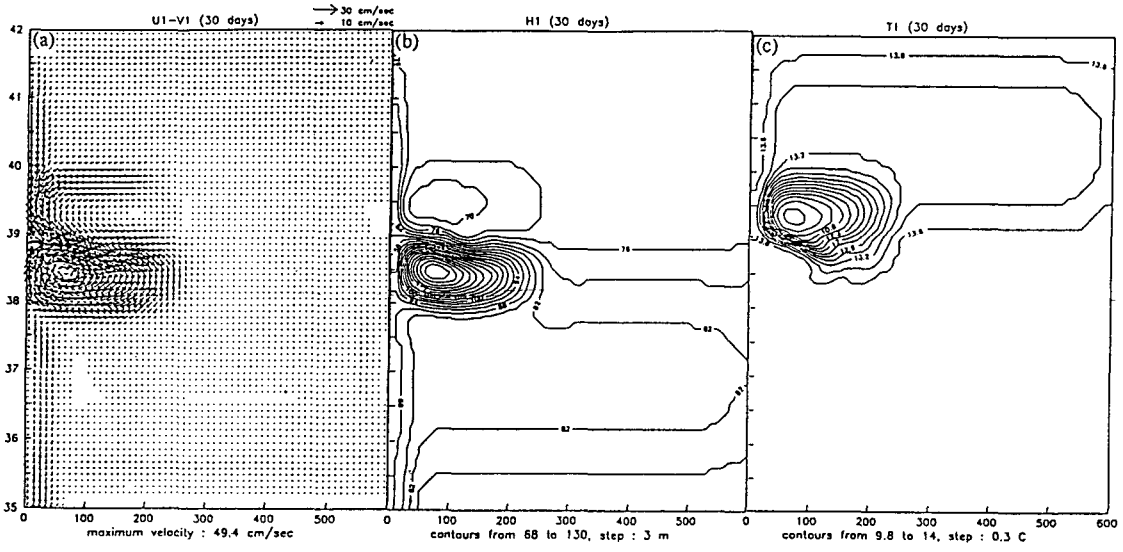

Fig. 6. A current field (a), h-field (b) and temperature field (c) of the upper layer at day 30.

maximum speed reaches 49.4 cm/sec (Fig. 6a). A weak cyclonic eddy is also formed on the left side of the wind axis, but it disappears due to entrainment after day 60. The elimination of the cyclonic eddy will be discussed later in detail. The shallowing of the *h*-field to the left of the wind axis is much less than its deepening to the right (Fig. 6 b). Maximum thickness at the center of the anticyclonic eddy reaches about 130 m. Temperature decreases by entrainment in a broad region to the left of the wind axis (Fig. 6c). It reaches a minimum value of 9.8℃ at the center of the cyclonic eddy.

At day 45 (Fig. 7), the nonlinear advection and entrainment appear in the anticyclonic and cyclonic area, respectively. The most interesting feature is the lack of symmetry of the two eddies. The anticyclonic eddy is very strong and starts to be in

a circular shape, and its maximum speed reaches 62.2 cm/sec, whereas the cyclonic eddy considerably weakens. The southward current also weakens compared to that at day 30 (Fig. 7a). All the regions where h is less than H vanish because of entrainment, so that the cyclonic eddy almost disappears. Maximum thickness reaches 173 m at the center of the anticyclonic eddy (Fig. 7b). Temperature decreases due to entrainment by Ekman pumping and its minimum value drops from 9.8℃ at day 30 to 8.9℃ at day 45 (Fig. 7c). Tongues of both cold and warm waters begin to advect around the anticyclonic eddy.

At day 60 (Fig. 8), the anticyclonic eddy of about 180 km in diameter becomes completely circular due to the nonlinear advection. Its maximum speed decreases to 43.4 cm/sec because the strong offshore winds stops, and its center (Xm, Ym) is located near Xm=100 km, Ym=38.2 N. A weak eastward meandering current from the eastern side of the anticyclonic eddy is also developing. The reason why the meander is generated in the eastward current will be explained later. The southward coastal current along the western boundary considerably weakens and nearly disappears on the southern part of the anticyclonic eddy (Fig. 8a). The cyclonic eddy is completely removed and maximum thickness at the center of the anticyclonic eddy reaches 169 m (Fig. 8b). Thickness between 36 °N and 37°N reaches about 92 m. Temperature

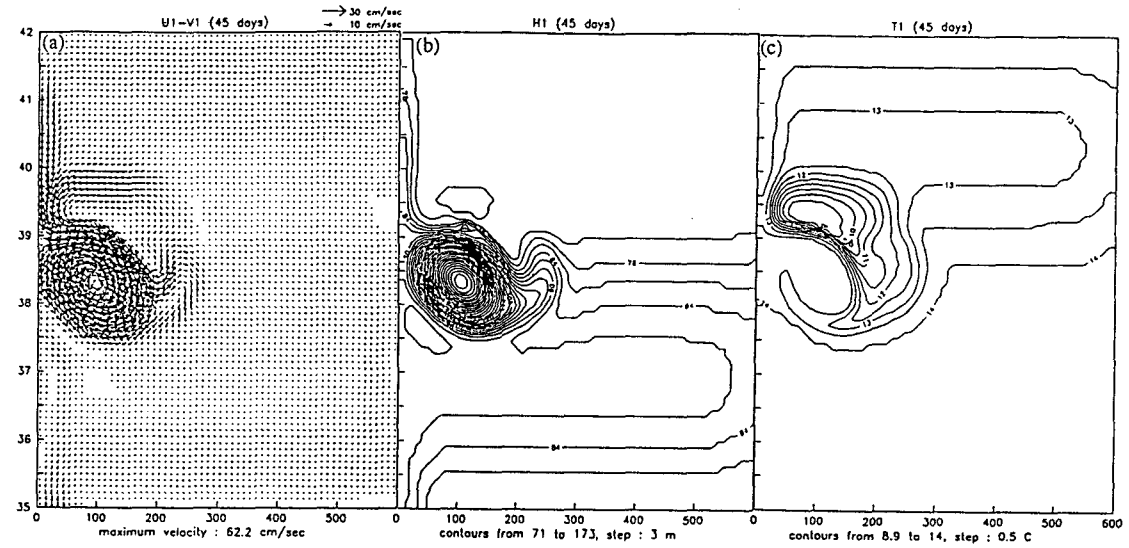

Fig. 7. A current field (a), h-field (b) and temperature field (c) of the upper layer at day 45.

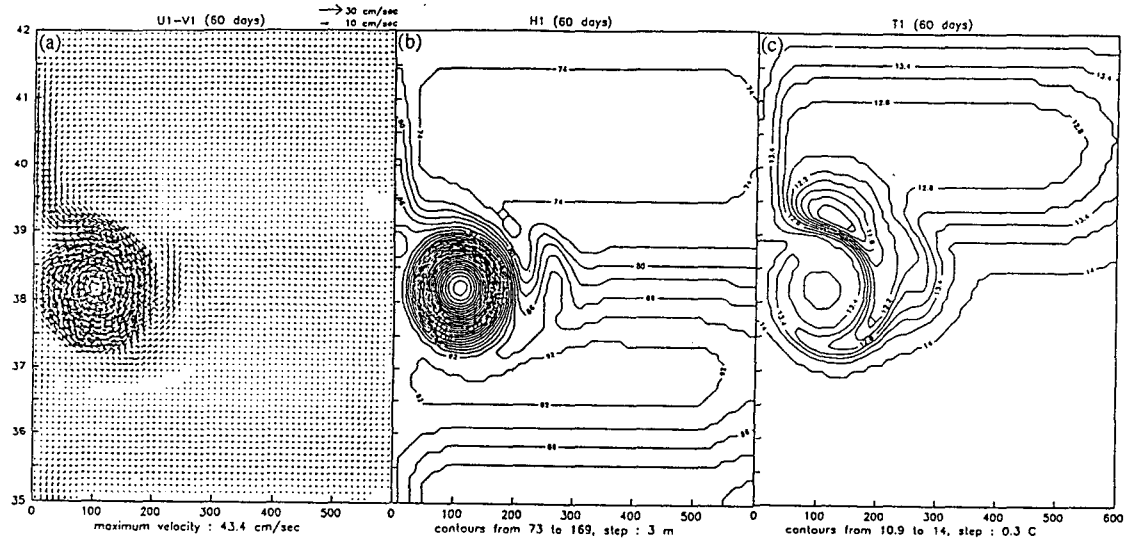

Fig. 8. A current field (a), h-field (b) and temperature field (c) of the upper layer at day 60.

ranges from 10.9℃ to 14℃, and tongues of cold and warm waters wrapping around the anticyclonic eddy are clearly evident (Fig. 8c).

Fig. 9 shows the velocity field, thickness field and temperature field at day 90. The size of the anticyclonic eddy increases to about 200 km due to horizontal diffusion, but maximum speed decreases to about 38.0 cm/sec because of horizontal mixing. Maximum thickness of the anticyclonic eddy still remains about 163 m and its position is not changed. The eastward meandering is clearly shown and its speed increases to about 10 cm/sec. The southward coastal current completely disappears due to decaying of the northerly wind. Instead, the northward coastal current along the western boundary is generated to compensate the eastward displaced water on the right side of the anticyclonic eddy. Distribution of temperature is nearly similar to that at day 60, but minimum value rises to 12.4℃ because of heat flux Q (Fig. 9c).

The velocity field, *h*-field and temperature field at day 120 are shown in Fig. 10. Maximum speed is about 37.0 cm/sec. Although minimum value reaches 13.1℃, temperature is mostly restored to the surrounding water temperature of 14℃, so that the anticyclonic eddy seems to disappear in the temperature field. In fact, the anticyclonic eddy still remains and its maximum thickness at the eddy center reaches about 156 m. At day 180, the temperature field is not presented in this thesis, since temperature is nearly restored to 14℃. The coastal current along the western boundary flows to the north like that at day 90, and it continues to flow by day 360 with a speed of 10 cm/sec and a width of 70 km. Thickness of the upper layer decreases to the left side of the current due to the thermal wind relation.

In this offshore winds study, the anticyclonic eddy is transformed into an elliptical shape in meridional direction due to western boundary. To examine the cause of change in the shape of eddy and the northward movement of eddy in detail, we carried out various additional calculations. Anticyclonic eddies were created artificially in the central part of the model ocean to allow enough space for the eddy to move. First, the propagation speeds of eddies were investigated. Mean propagation speeds of eddies increased in proportional to size and strength of eddies. All eddies propagated westward and their mean propagation speeds were over 0.5 km/day. With time, mean propagation speeds decreased and eddy size increased due to horizontal diffusion. Compared with this offshore winds study, the most remarkable difference was that the circular eddies changed into an elliptical shape not in meridional direction but in zonal direction with time. As a result, the strong anticyclonic eddy in this offshore winds study seemed to be transformed into an elliptical shape in meridional direction because its westward movement was prevented by the western boundary. Lee et al. (1995) traced the Sogcho Eddy from January to June 1992 using the AVHRR imagery. The Sogcho Eddy was approximately circular in earlier stage (January), but it became elongated along the east coast of Korea later (February).

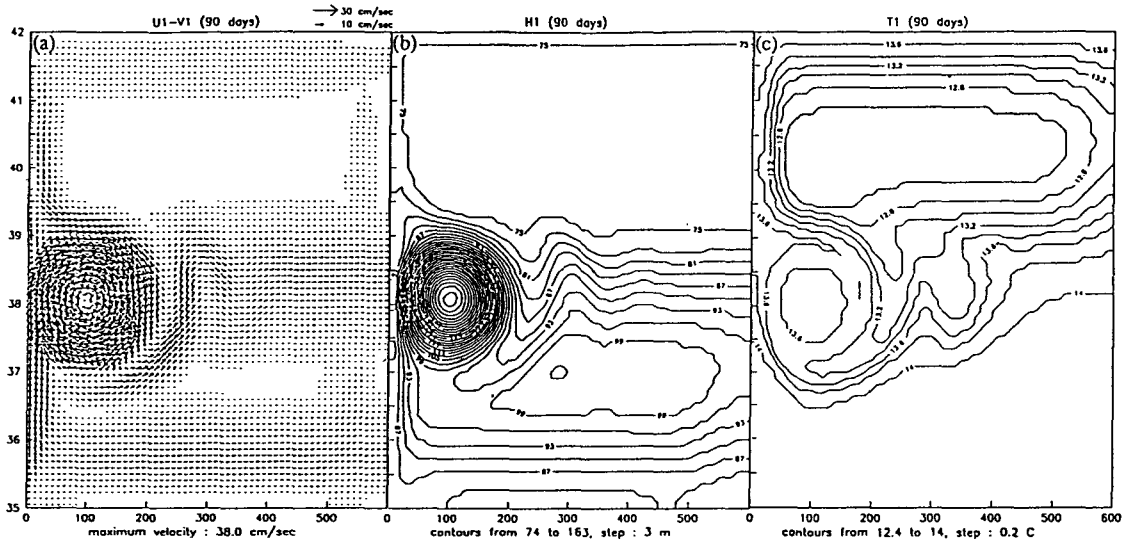

Fig. 9. A current field (a), h-field (b) and temperature field (c) of the upper layer at day 90.

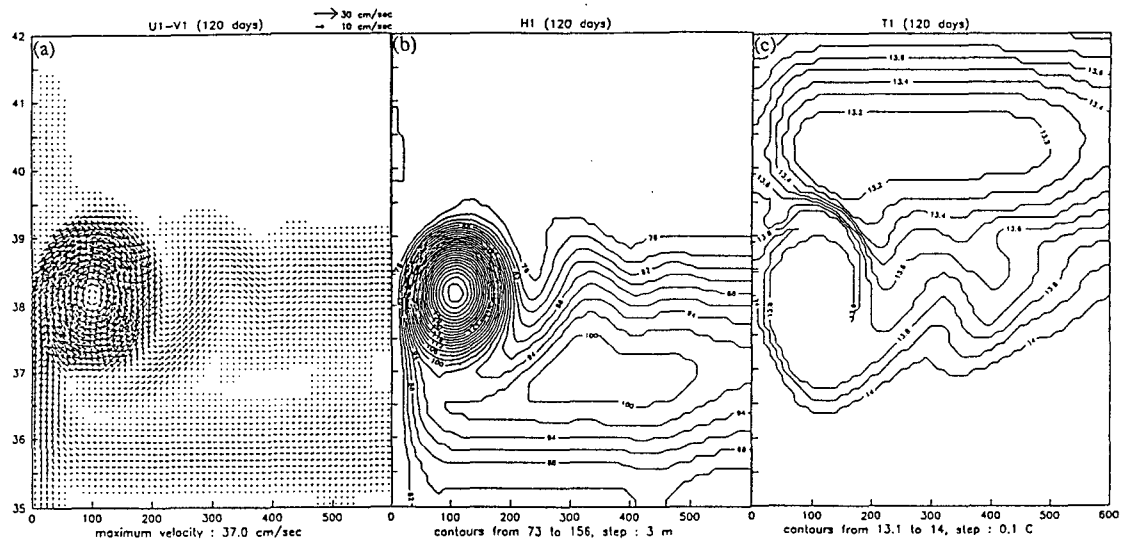

Fig. 10. A current field (a), h-field (b) and temperature field (c) of the upper layer at day 120.

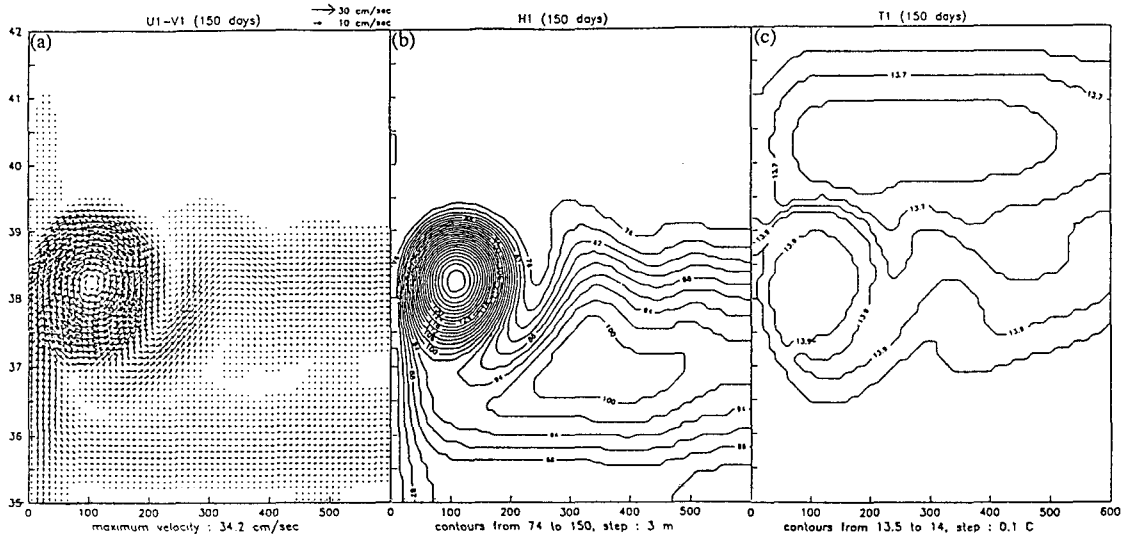

Fig. 11. A current field (a), h-field (b) and temperature field (c) of the upper layer at day 150.

The velocity field, *h*-field and temperature field at day 150 (Fig. 11) and 360 (Fig. 12) are almost similar to those at day 120 (Fig. 10). The anticyclonic eddy slowly move to the north with time. Meandering motion of the eastward current is evident, and its wavelength increases to about 160 km at day 150. After 360 days it increases to about 230 km. According to the results of various additional calculations, as the eastward meandering current became stronger, its wavelength also increased. Temperature ranges from 13.5℃ into 14.0 ℃ (Fig. 11c), but temperature is mostly restored to the surrounding water temperature with time. The velocity and thickness fields show the existence of an anticyclonic eddy attached to the western boundary by day 360, and also show that the northward coastal current and eastward meandering current continue to flow by day 360. Presumably, the anticyclonic eddy and meandering motion generated by the wind forcing would have remained for one year without any other external forcing.

The major current systems with meandering motion and eddies in open ocean have been studied many oceanographers. McCreary and Kundu (1988) studied meandering motion and eddies particularly in Somali Current System during the Southwest Monsoon. They proposed that a western boundary current was developed by the response to the southern hemisphere easterlies, and that meanders were formed by the overshooting of the northward

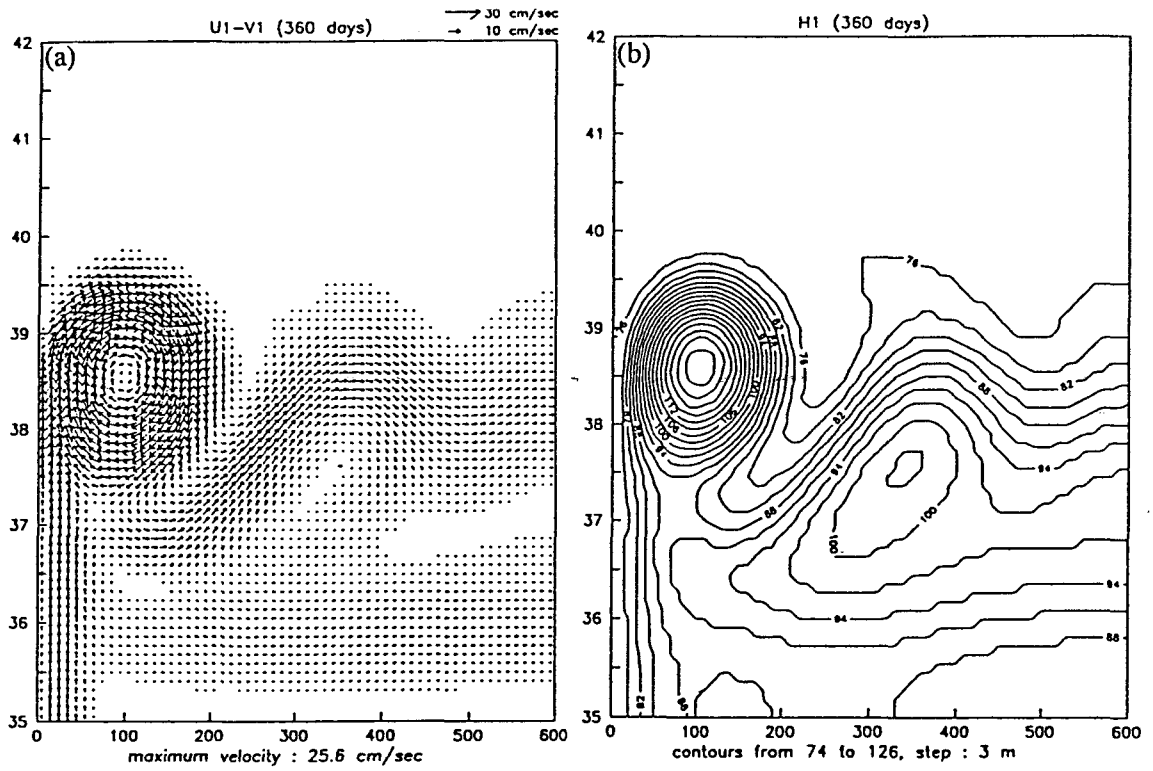

Fig. 12. A current field (a) and h-field (b) of the upper layer at day 360.

current near the coast, and then gradually spread out into the interior ocean. They showed that after the northward western boundary current became strong enough for the nonlinear effect to affect its own path, it overshot, that is, the boundary current acquired positive potential vorticity in order to join the eastward interior current. Horizontal friction in the western boundary was a strong source of positive vorticity. Thus, the water parcel remained in the boundary current until it acquired the necessary amount of positive potential vorticity, and the boundary current overshot if necessary, then the meanders began to form near the coast. According to their explanation, the meanders are akin to stationary Rossby waves, for which the westward phase speed is balanced by an eastward current, and the meanders gradually spread out into the interior ocean because the stationary Rossby waves have eastward group velocity.

In this offshore winds study, the eastward meandering current was developed on the eastern side of the strong anticyclonic eddy after 60 days. Now, we explain how the meander develops. The anticyclonic eddy generated in this study seems to be the stationary Rossby waves similar to the study of McCreary and Kundu (1988). The energy of Rossby waves propagating to the west have been deflected to the east at the western boundary, so that the meander seems to have been generated on the right side of anticyclonic eddy. Since the short Rossby waves having eastward group velocity dissipate easily, the meander will not propagate longer.

The center of eddy (Xm, Ym) also shifts from $Xm=100$ km, $Ym=38.2$ N at day 60 to $Xm=100$ km, $Ym=38.6$ N at day 360, which yields a northward mean drift for 300 days of about 0.15 km/day. To investigate the characteristics of northward movement of eddy, we also carried out various additional calculations. When the initial temperature of the upper layer was increased to 17 ℃, the velocity and size of the eddy increased accordingly (not shown). The velocity of the eastward meandering current, its wavelength and velocity of the northward coastal current also increased to about 13 cm/sec, over 250 km and about 15 cm/sec, respectively. The northward mean drift also increased to about 0.25 km/day. Lee (1990) suggested that the mean drift of anticyclone was enhanced by the background advection due to the secondary current driven by the wind. In additional calculation, the increased northward drift of the anticyclonic eddy seemed to be associated with both the increased speed of the northward coastal

current and the circulation speed of eddy. When the northerly wind continued to blow by day 360, the anticyclonic eddy did not move to the north because of southward coastal current. Therefore, the northward movement of the Sogcho Eddy seems to be associated with the strength of the North Korea Cold Current in the real East Sea.

We also carried out another additional calculations with only the northerly wind and background wind without a wind patch in the offshore direction. In that case, an eastward meandering current was developed, but a strong anticyclonic eddy was not generated near the western boundary. Only a semi-enclosed anticyclonic eddy was generated due to the overshooting of the coastal current near the western boundary. Therefore, the strong offshore winds are necessary for the strong and circular anticyclonic eddy to develop.

For this offshore winds study, the cyclonic motion was eliminated by entrainment like in McCreary et al. (1989). In this section, a physical process of the elimination of the cyclonic eddy is discussed in terms of the conservation of potential vorticity under the influence of entrainment.

In order to obtain a simple equation of the conservation of potential vorticity as McCreary derived (not published), the model ocean is assumed to be an inviscid, nonlinear 1½ - layer model including entrainment and it is forced by only a meridional wind field (τ^y). The conservation of potential vorticity for this case is

$$\frac{D}{Dt}\frac{(f+\zeta)}{h}=-W_e\left(\frac{f+\zeta}{h^2}\right)+\frac{\tau^y{}_x}{h} \tag{3.1}$$

Equation (3.1) means that positive entrainment velocity (W_e) is a sink of potential vorticity.

If there is neither wind forcing ($\tau^y=0$) nor entrainment ($W_e=0$), then equation (3.1) becomes

$$\frac{D}{Dt}\frac{(f+\zeta)}{h}=0, \tag{3.1}$$

so, the potential vorticity is

$$\frac{f+\zeta}{h}=\text{constant}. \tag{3.2}$$

Equation (3.2) means that water column conserves their potential vorticity. If h varies in time, relative vorticity (ζ) should be change to conserve potential vorticity. If h increases on the f - plane, the column gains positive relative vorticity.

In 1990, McCreary showed that entrainment sank potential vorticity in the model ocean (not published). In his model ocean, a linear, geostrophic and 1½ - layer model having a meridional wind patch and entrainment on the f - plane was assumed in order to understand entrainment effect easily. In that case, two - counter rotating eddies were generated on both sides of the wind axis due to the meridional wind patch. Because there is a vorticity gain due to the wind events on the f - plane, h has to weaken to sink potential vorticity and then relative vorticity decreases. Now, we must investigate changes of h at the two - counter rotating eddies. For this simple linear case, equations of motion are

$$-fv+g'h_x=0 \tag{3.3}$$

$$fu+g'h_y=\frac{\tau^y}{H} \tag{3.4}$$

$$h_t+H(u_x+v_y)=W_e \tag{3.5}$$

where $\begin{cases}\tau^y=\tau_0X(x)Y(Y)\delta(t), \\ W_e=-r(h-H), \qquad r=r_0\theta(H-h).\end{cases}$

Because entrainment (W_e) is assumed to be a step function (where θ is a step function), entrainment is given only where h is shallower than H. After changing equations (3.3) and (3.4) into equation (3.6) to obtain h - equation, plug equation (3.6) into equation (3.5), then we get equation (3.7)

$$v_y=\frac{g'}{f}h_{xy} \quad \text{and} \quad u_x=\frac{-g'}{f}h_{xy}+\frac{1}{fH}\tau^y{}_x, \tag{3.6}$$

$$h_t+\frac{\tau_0}{f}X_xY\delta(t)=r_0(H-h)\theta(H-h). \tag{3.7}$$

Where h is shallower than H ($h<H$), we take the Laplace Transform to equation (3.7), after this, we take an inverse Laplace Transform, then equation (3.7) becomes

$$h=H-\frac{\tau_0}{f}X_xY_e^{-r_0t}\theta(H-h). \tag{3.8}$$

Where h is deeper than H ($h>H$), equation (3.7) changes to

$$h=H-\frac{\tau_0}{f}X_xY\theta(h-H). \tag{3.9}$$

Therefore, h at the two-counter rotating eddies is

$$h=H-\frac{\tau_0}{f}X_xY\theta(-X_x)-\frac{\tau_0}{f}X_xY_e^{-r_0t}\theta(X_x) \tag{3.10}$$

Equation (3.10) shows that only cyclonic eddies

(third term) weakens in time. With this switched form $[\theta(h\text{-}H)\rightarrow\theta(-X_s)]$ of entrainment, the solution adjusts to a state with a single anticyclonic eddy and the system has lost positive relative vorticity due to positive entrainment velocity (W_e). Therefore, entrainment can act to eliminate the cyclonic eddy in the nonlinear solution. In addition, the disappearance of the eddy does not violate the principle of the potential vorticity conservation. As a result, if the model ocean is forced by the wind patch (either τ^y or τ^x), the anticyclonic and cyclonic eddies can be generated on both sides of the wind axis, but the cyclonic eddy needs to be removed in time by entrainment effect where h is shallower than H. Then, a stronger anticyclonic eddy can develop on the right side of the wind axis and can last longer. Consequently, the strong anticyclonic Sogcho Eddy of about 200 km in diameter could be generated by the strong offshore winds prevailing in the Kangnung - Sogcho regions in winter season. But, the cyclonic eddy was not clearly observed.

Summary and Conclusions

To investigate the mechanism of the generation of the Sogcho Eddy, we carried out numerical experiment using the nonlinear 1½ - layer model with the strong offshore winds and the background winds.

The analysis of wind data at Sogcho, Kangnung and Samchuk showed that the wind was stronger in winter than in other seasons and the offshore component was dominant. Particularly the strong offshore winds from December 1991 through February 1992 were considered to be favorable for the generation of the Sogcho Eddy observed in 19 92. The influence of strong offshore winds on the generation of the Sogcho Eddy was investigated in this offshore winds study. An anticyclonic eddy of about 200 km in diameter was generated due to the intense offshore winds near the western boundary. The anticyclonic eddy transformed into an elliptical shape in meridional direction because of the blocking effect of the western boundary.

The meander was also developed in the eastern side of the eddy due to the eastward propagation of the Rossby wave energy reflected at the western boundary. After 90 days, when the offshore winds decayed, a northward coastal current with speed of 10 cm/sec was induced to compensate the eastward meandering current. The anticyclonic eddy moved to the north with mean drift of about 0.15 km/day, and it seemed to be accelerated by the northward western boundary current.

With the results of the polar front study (Kim et al., 1997b), and this offshore winds study, we concluded as follow; The Sogcho Eddy might be generated by the existence of the polar front near the western boundary (Kim et al., 1997b), but the results of the offshore winds study showed that the strong offshore winds could generate a larger and stronger eddy than the one caused by the baroclinic instability. Therefore, the Sogcho Eddy may be produced by the combined effects of the polar front near the western boundary and the strong offshore winds. Also, we can expect that the size of the Sogcho Eddy will be smaller when it is generated only by the baroclinic instability, whereas it will be greater and getting circular shape while being affected by the strong offshore winds. But, in this study we are not sure which mechanism for the generation of the Sogcho Eddy is most important. For the theoretical and, more importantly, observational studies are needed.

References

Choi, H. and Y. K. Lee, 1993. A study on the characteristics of Tonghae coastal winds. Ocean Research, 15, 1~13 (in Korean).

Kim, S. Y., J. C. Lee, H. S. Lee and T. B. Shim, 1997a. Numerical Experiment on the Ulleung Eddy due to the variation of the Tsushima Current in the East Sea. J. Korean Fish. Soc. (submitted).

Kim, S. Y., J. C. Lee, H. S. Lee and T. B. Shim, 1997b. Triggering effect of the polar front on the eddies in the East Sea. J. Korean Fish. Soc. (submitted).

Lee, H. S., 1990. The coastal ocean response to strong offshore winds in the Gulfs of Theuantepec and Papagayo. Ph. D. thesis, Nova University, Dania, 116 pp.

Lee, J. C., D. H. Min, T. B. Shim, H. S. Lee and H. S. Yang, 1995. The Sogcho Eddy, I: Observation on May 1992.. J. Kor. Fish. Soc., 28, 354~364.

McCreary, J. P., H. S. Lee and D. B. Enfield, 1989. The response of the coastal ocean to strong offshore winds : With application to circulation in the Gulfs of Tehuantepec and Papagayo. J. Mar. Res., 47, 81~109.

McCreary, J. P. and P. K. Kundu, 1988. A numerical investigation of the Somali Current during the southwest monsoon. J. Mar. Res., 46, 25~58.

Na, J. Y., J. W. Seo and S. K. Han, 1992. Monthly mean sea surface winds over the adjacent seas of the Korea Peninsular. J. Oceanogr. Soc. Korea, 27, 1~10.